GiG Research Institute

JOURNAL OF SUSTAINABLE MINING

Volume 21 | Issue 4 Article 6

2022

Quantifying the Influence of Variations in Rock Mass Properties on Stope Stability

Author(s) ORCID Identifier:
Shahé Shnorhokian: 0000-0002-4001-4779
Hani Mitri: 0000-0002-6482-7424

Quantifying the Influence of Variations in Rock Mass Properties on Stope Stability

Abstract

Variations in rock mass properties are well-established in rock mechanics and underground mining. The literature is replete with methods of assessing them and determining values that are used in design or numerical analysis. In this paper, a simplified 3D model is constructed for a tabular orebody in the Canadian Shield and instability is quantified using the ”brittle shear ratio” criterion to calculate the volume at risk. A 1-4-7 stope pillar sequence is implemented on four active levels, and three variations in the properties of the host formation are assessed. It is observed that the locations of ore at risk follow the formations of stope pillars and are then transferred to the sill pillars above and below. Instability in the footwall and the hanging wall is observed to be lesser in volume but remains persistent. With the allocation of weak properties to the host rock, at-risk volumes increase in the orebody, footwall, and hanging wall, and the reverse trend occurs with strong greenstone properties. It is concluded that the stress increase in the orebody is due to transfers from the weaker host rock, while that in the greenstone formation is due to the use of a lower compressive strength value.

Keywords

stope stability, rock mass variations, numerical modelling, footwall stability, volumetric analysis, brittle shear ratio

Quantifying the Influence of Variations in Rock Mass Properties on Stope Stability

Shahé Shnorhokian*, Hani Mitri

McGill University, Department of Mining and Materials Engineering, Canada

Abstract

Variations in rock mass properties are well-established in rock mechanics and underground mining. The literature is replete with methods of assessing them and determining values that are used in design or numerical analysis. In this paper, a simplified 3D model is constructed for a tabular orebody in the Canadian Shield and instability is quantified using the "brittle shear ratio" criterion to calculate the volume at risk. A 1-4-7 stope pillar sequence is implemented on four active levels, and three variations in the properties of the host greenstone formation are assessed. It is observed that the locations of ore at risk follow the formations of stope pillars and are then transferred to the sill pillars above and below. Instability in the footwall and the hanging wall is observed to be lesser in volume but remains persistent. With the allocation of weak properties to the host rock, at-risk volumes increase in the orebody, footwall, and hanging wall, and the reverse trend occurs with strong greenstone properties. It is concluded that the stress increase in the orebody is due to transfers from the weaker host rock, while that in the greenstone formation is due to the use of a lower compressive strength value.

Keywords: stope stability, rock mass variations, numerical modelling, footwall stability, volumetric analysis, brittle shear ratio

1. Introduction

Sublevel open stoping with delayed backfill is a common underground extraction method widely used in mines in Canada and elsewhere [1,2,3]. The basic requirements for the general method are a steeply dipping tabular orebody having clear boundaries with the host rock mass and geologic formations that have moderate strength properties [4]. It comprises multiple variations in which different types of temporary pillars are formed that are eventually extracted. Horizontal pillars are designed to separate mining blocks along the orebody depth, and vertical ones serve to separate between primary, secondary, or tertiary stopes. Depending on the adopted mining sequence, pillar locations and extraction time vary, affecting induced stress concentration and magnitude [4]. Stope sequencing is, therefore, vital to provide maximum safety and operational efficiency [2,5]. A calibrated numerical model can be combined with engineering criteria used for underground design to examine the potential for instability for the various sequence alternatives being considered in a relatively short period of time [5,6,7]. An advantage of using a failure criterion in 3D models is the ability to quantify both the volume of the rock mass that has been excavated and the one designated to be "at risk" in all axis directions for each mining stage, which allows for a comparison between the different options available.

As an underground mining method, sublevel stoping requires competent rock mass properties and the presence of pillars, which result in ground control challenges such as rock bursting and mining-induced seismicity. This has been established through the bilinear failure envelope [8,9,10,11], where a zone of microseismicity exists at deviatoric stress ($\sigma_1-\sigma_3$) values plotting above the damage threshold. Castro et al. [5] designated a ratio of the deviatoric stress to the unconfined compressive strength (UCS_i) of the intact rock exceeding 0.35 as

Received 20 April 2022; revised 27 July 2022; accepted 1 August 2022.
Available online 18 November 2022

* Corresponding author.
E-mail address: shahe.shnorhokian@mcgill.ca (S. Shnorhokian).

https://doi.org/10.46873/2300-3960.1368

the initiation of rock mass damage, with 0.7 defined as the threshold for major strain bursting. This is often referred to as the "brittle shear ratio" (*BSR*) and has been used by the industry as a design criterion for stope sequence options [12,13] and geometrical parameters such as stope dimension and dip [14].

When a certain mining method is combined with numerical modelling, multiple stope sequence options can be examined before a final strategy is adopted. Villaescusa [3] conducted an extensive review of those used specifically in sublevel open stoping. Others [1,2,15,16,17,18] provided in-depth reviews of typical sequences used at Canadian mines. FLAC3D was used for extraction optimization at the Eleonore mine [19], and for studying its impact on stope stability at the Niobec mine [13]. Examine2D and RS3 were adopted to study the extraction sequence in the Upper Orebody at the Nchanga mine in Zambia [20]. The use of dip stabilizing pillars in deep reef mining in South Africa was also studied using numerical modelling, comparing a new multi-raise sequence to the traditional sequential grid mining approach in terms of production rates and microseismic effects [21,22]. In Australia, the implementation of a 1-5-9 sequence at the George Fisher mine [23], a 1-3-5 one at the Kanowna Bell Gold Mine [24,25], and a chequer-board pattern in the 1100 Orebody at Mount Isa Mines were reported [26]. An overview of techniques used in Western Australian mines to manage challenging stress-related instability was also provided [27]. Another study was conducted there for a diminishing pillar sequence in the Mist orebody at the Frog's Leg mine [28]. In Scandinavia, 3DEC was used to examine stope sequences that would minimize fault slip in Block 19 of the Kiirunavara mine [29].

While modelling different sequence options is a useful tool for mine planning, another challenge that must be overcome is the heterogenous nature of geologic formations and the spatial variations in their properties. Distribution ranges of laboratory results on rock samples and in-situ rock mass parameters are well-established in the literature. There are several statistical techniques that have been developed specifically for geomechanical applications [30,31,32,33,34] or used in rock mass classification schemes [35,36,37,38]. These variations need to be addressed at the preliminary and final design stages in mining [32,39,40,41], as well as in any numerical modelling analyses [13,42,43,44]. Furthermore, the subject automatically leads to the concept of reliability-based design and the availability of statistically sufficient data for intact rock and discontinuities to generate a synthetic equivalent of the rock mass [45]. Two common approaches specifically used in modelling comprise probability density functions (PDFs) of various properties combined with Monte Carlo simulations [30,33,46,47,48,49] or the mean value for each parameter based on their individual statistical distributions [50].

A third but less commonly used method is to run the model with different rock mass property inputs and to assess their impact on instability. Geostatistical tools such as variograms, Kriging, and frequency distributions were used to develop a 2D model of the rock mass at the Masua mine, including variations in discontinuity properties [39]. A tunnel/cavern stability analysis was also conducted with Phase2 (currently RS2) using PDFs of intact rock test results, GSI values, and the Monte Carlo method [40]. The unique outcome of this study was the probability distribution of yielding zones and total displacements around the underground opening, which allowed the design of an appropriate rock support system. In another study, the extent of yielding zones and displacements were determined for roadway B-7 at the Pniówek coal mine with four simulations representing the median, average minus standard deviation, average minus statistical error, and average rock mass properties [51]. In 3D studies, a geological model was developed for a system of twin tunnels in Greece where Kriging was used to incorporate the rock mass rating (*RMR*) value into the model and analyze it using FLAC3D [52]. This code was also used in the analysis of a tunnel supported by steel arches at 1000 m depth with variability coefficients describing the distribution of rock mass properties [53]. After running 13 simulations with different properties, the authors assessed their impact on the overall stress, plasticization, and forces in the support elements. Extensive research on the impact of variations in rock mass properties on underground mine stability has been carried out in Sweden. A conceptual 2D model of a steeply dipping orebody was constructed in FLAC and extracted using the sublevel stoping method, where the impact of rock mass property PDFs was assessed on the final probability distribution of stope wall convergence and tangential stresses [54,55]. The authors then conducted a separate study with the same code on a primary-secondary stope extraction sequence with a different orebody and host rock geometry, evaluating roof sag and floor heave in addition to wall convergence [56]. The PDFs of various geologic formations were analyzed for the Malmberget mine using their Mohr-Coulomb and Hoek–Brown

properties [33]. Pillar stability at the Laisvall mine was stochastically assessed using artificial neural networks with rock mass properties and the in-situ stress regime through FLAC3D modelling [57]. In recent years, detailed studies on stope stability under the influence of variations in geometry and rock mass properties were also conducted for the Niobec mine in Quebec. The effects of stope, size and inclination values for a mine in the Canadian Shield were generated using a Monte Carlo simulation, and overall stability was assessed using FLAC3D [13]. The authors also conducted a study at the same mine in which PDFs of intact rock and rock mass properties and their effects on the probability of failure (PoF) in compression or tension were assessed [13,44]. In a second study at the Niobec mine, the uncertainties of in-situ stress magnitudes were evaluated using Taylor's statistical method [58]. A final example of a 3D analysis of rock mass properties and their impact on instability was the use of a simplified model of another case study mine in the Canadian Shield [59]. The authors divided the properties into weak, average, most likely, and strong, and then analyzed the impact of 31 variations in individual and group formations on the pre-mining stress regime.

Analysis of the variations in rock mass properties and multiple sequence alternatives in a mining block is a complex undertaking that can only be conducted through numerical methods. To simplify comparisons between the available options, an instability criterion needs to be combined with volumetric analysis to identify the location and timing of potential ground control issues at each stage. In this study, a simplified model of a steeply dipping, tabular deposit within the Canadian Shield is constructed in FLAC3D, and rock mass properties and in-situ stress tensors typically found in this geologic province are used as input parameters. Previously, three stope sequence alternatives were simulated using diminishing, 1-4-7, and 1-5-9 pillar strategies for a total of 144 stopes. It was concluded that a 1-4-7 sequence incurred more instability on the active levels and in the footwall than the others, using a combination of the *BSR* criterion and volumetric analysis [60]. The same combined approach is used in this paper for the 1-4-7 sequence to examine the impact of variations in rock mass properties on instability in the orebody, footwall, and hanging wall and on the active levels at each stage of mining.

2. Numerical model

The orebody in the simplified model constructed in FLAC3D extends for 360 m along an E-W strike and dips 80° to the south. The host formations comprise metavolcanics with a dominant greenstone formation, a stiff norite unit to the north, and metasediments to the south. A swarm of igneous intrusions in the region is represented by two dykes striking WNW-ESE to the north and south of the orebody. The model dimensions are 840 m along the E-W axis, 390 m along the N-S one, and 300 m in depth. A total of 862,400 zones are used with a higher mesh density in the regions of interest. Based on commonly used intervals in sublevel open stoping, vertical distances between levels are set at 30 m. Stopes are dimensioned at 20 m along the strike length, 15 m in width, and 30 m in height, translating into 18 stopes longitudinally and two transversely for a total of 36 on each level. Mining is simulated from the bottom up on four active levels – L1550, L1520, L1490, and L1460 – at a depth of 1550–1430 m. Each stope is designed to comprise a volume of 9000 m^3 for a total of 324,000 m^3 per level and 1,296,000 m^3 on all four active levels. Haulage drifts are excavated in the footwall at 30 m from the orebody, in addition to three crosscuts per level – western, central, and eastern. Drift and crosscut dimensions are based on those typically used in Canadian mines with a 5 m × 5 m cross-section and a 1-m arch in the back. Fig. 1a presents an isometric view of the model and Fig. 1b provides a plan view on L1490. The mining block from L1580 to L1430 is shown in detail in Fig. 2a, viewing it from the southwest, while the specifics of haulage drifts and crosscuts are presented in Fig. 2b, viewing them from the west. The rock mass properties used in the model are based on a previous case study mine in the Canadian Shield. Laboratory test results on intact rock samples are combined with borehole logs indicating the rock mass rating (*RMR*) to derive the required rock mass properties to be used as input parameters. These are categorized into average, weak, and strong for each geologic formation, and the model is initially run with the average values for all units. Two additional simulations are run with weak and strong properties only for the greenstone formation that hosts the orebody, to assess the impact on instability in the orebody, footwall, and hanging wall.

The rock mass properties for all geologic formations and the two additional variations are summarized in Table 1. Intact rock properties such as Young's modulus E_i, Poisson's ratio ν, and uniaxial compressive strength UCS_i are presented, in addition to rock mass properties such as rock mass rating *RMR*, deformation modulus E_{rm}, bulk modulus *K*, and shear modulus *G*. The model is simulated in linear elastic mode to maximize induced stress

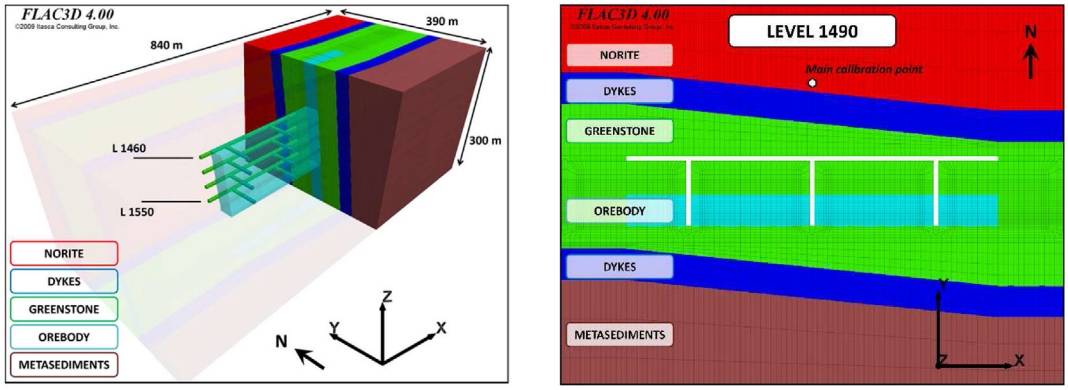

Fig. 1. (a) Isometric view of the mining block, development network, and host rock formations; (b) Location of main in-situ stress calibration point in the norite formation on L1490.

magnitudes and provide a more conservative estimate of potential instability. Based on the rock mass properties of the geologic units, the "brittle shear ratio" (*BSR*) criterion is selected to gauge the potential for instability in the orebody and greenstone formation, which constitutes both the footwall and hanging wall. The generation of pre-mining stresses in the heterogeneous rock mass is achieved using boundary tractions applied on all sides of the model [61]. Calibration is conducted by obtaining model readings on L1490 within the norite formation comparable to in-situ measurements at the previous case study mine, as shown in Fig. 1b. Additional model readings at the same location on L1400 and L1580 are compared to typical stress rate increases measured in the Canadian Shield [62,63]. Table 2 presents a comparison of the in-situ measurements and model stress readings along the directional axes. The only significant shear stress component measured in the field is σ_{xy}, which reads between 8.5 and 9.6 MPa on the three levels. This is very closely matched by the model readings that also vary between 8.74 and 9.42 MPa at the same locations.

The stope sequence implemented within the mining block from L1550 upwards to L1460 is a 1-4-7 approach whereby the first, fourth, seventh, tenth, thirteenth, and sixteenth stopes on each active level are designated as primary ones. After their extraction and backfilling, stopes 2-5-8-11-14-17 are mined as secondaries and finally, stopes 3-6-9-12-15-18 are extracted as tertiaries. The stope sequence is implemented with a lag of at least two levels between primaries-secondaries and secondaries-tertiaries, and this is visually presented in Fig. 3. Each mining stage represents the extraction of six stopes from various locations within the four active levels and a total of 24 stages are simulated with 6 stopes per stage, resulting in 144 stopes being extracted.

Due to the relatively competent nature of both host rock and orebody, the *BSR* is adopted as the

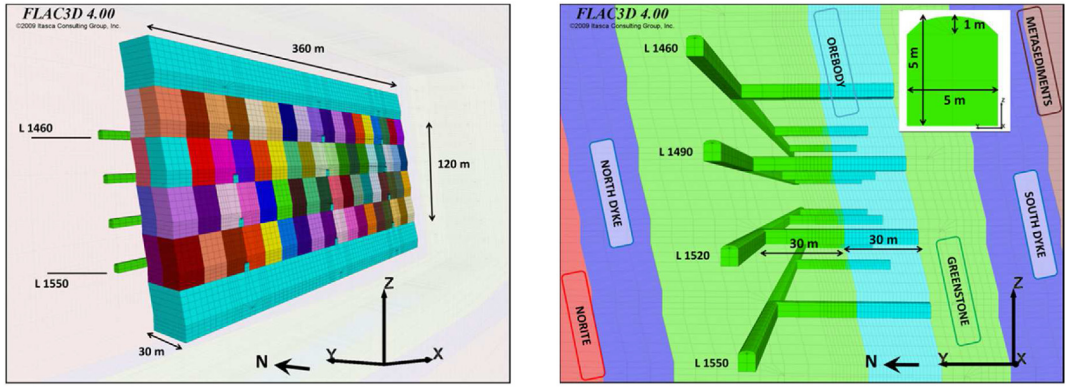

Fig. 2. (a) Stopes on the four active levels between L1550 and L1460 with sill pillars on L1580 and L1430; (b) Details of the haulage drift and crosscuts on the four active levels.

Table 1. Rock and rock mass properties of geologic formations.

Geological unit	E_i (GPa)	ν	UCS_i (MPa)	*RMR*	E_{rm} (MPa)	*K* (MPa)	*G* (MPa)
Dyke	126	0.24	224	63	58,816	37,703	23,716
Norite	177	0.21	201	59	69,234	39,790	28,609
Metasediments	77	0.29	183	55	23,127	18,355	8964
Orebody	69	0.30	138	75	50,564	42,137	19,448
Greenstone							
Average	79	0.26	178	60	31,829	22,103	12,630
Strong	149	0.24	268	80	120,523	77,258	48,598
Weak	55	0.20	101	48	10,586	5881	4411

instability criterion in this study. A value of 0.7 is used as the threshold above which rock mass is considered to be "at risk" as it becomes a source of intense induced seismicity. To render a more conservative analysis, the properties of rock mass attaining a threshold of 0.7 in a mining stage are not reduced in the following one, and, therefore, a strain-softening constitutive model is not used in the simulation. The *BSR* is combined with volumetric analysis to conduct a quantitative comparison of unstable or "at risk" rock mass. The orebody, footwall, and hanging wall are monitored separately in each mining stage, and the volume of unstable rock mass within each domain is recorded to detect any changes in values. The cumulative volume is compared in each stage to observe their impact on stability on individual levels in the orebody, footwall, and hanging wall.

3. Results and discussion

An overall comparative analysis is first conducted for the volume of unstable rock mass above a *BSR* of 0.7 for all active levels, as well as L1580 below and L1430 above. This is done for the orebody, footwall, and hanging wall, where average rock mass properties are initially used for all geologic formations. Secondly, a single active level with a relatively large volume of instability is selected and compared to simulation results, where the greenstone formation is first given weak and then strong rock mass properties. Finally, the overall rock mass at risk in the orebody, the footwall, and the hanging wall is quantitatively compared amongst the three variations in greenstone properties.

3.1. Average rock mass properties

3.1.1. Orebody

The timing of instability within the orebody is linked to the 1-4-7 stope pillar sequence being implemented on the active levels. As shown in Fig. 4, the volume of ore at risk remains minimal throughout the sequence on L1550 and reaches a maximum of 12,081 m^3 in stage 12. This is because the slender pillars formed at this point extend from L1580 to L1430 and are still connected to the rest of the orebody, thus channelling part of the induced stresses towards the intact rock mass. By stage 14, all stopes on L1550 are extracted and backfilled, and the pillars on L1520 are unable to shed the stresses into the rock mass below. Hence, a significant increase in instability is observed on this active level, with the volume attaining 61,744 m^3. In stage 16, the first stopes are mined on L1460 while this volume reaches 64,510 m^3 on L1520. When all the ore is extracted there in stage 18, the increase in unstable volume is transferred upwards to L1490 and continues to increase to 75,893 m^3 in stage 20. The pattern is repeated with the depletion of ore on L1490 in stage 22, where 64,712 m^3 of unstable rock mass is observed on the uppermost active level. The values there are reduced to nil with the completion of mining for the entire block. Therefore, a clear trend emerges in that the volume of rock mass at risk moves sequentially from one active level up to the other based on the formation and removal of ore pillars. Furthermore, the analysis also indicates when, where, and for how long instability is to be expected on each active level. This is helpful for ground control engineers as they can plan the timing and duration of implementing appropriate ground control measures. In addition, while the *BSR* value in stopes exceeds 0.7 with the formation of pillars on an active level, it does not automatically translate into this volume being identical everywhere in the mining block, with L1520 and L1490 carrying the largest proportions of ore at risk for the longest durations. Lastly, while instability is no longer present at the end of mining on an active level, it increases continuously in the sill pillars on L1580 and L1430 and reaches approximately 95,000 m^3 on the former in stage 24. Hence, mining in those areas at a later

Table 2. Comparison of in-situ stress measurements and model predictions.

Norite formation	Target σ_{xx} (MPa)	Target σ_{yy} (MPa)	Target σ_{zz} (MPa)	Model σ_{xx} (MPa)	Model σ_{yy} (MPa)	Model σ_{zz} (MPa)
L1400	64.94	44.68	37.80	65.10	45.82	37.37
L1490	69.12	47.55	40.23	69.16	47.55	40.26
L1580	73.29	50.42	42.66	72.85	49.79	43.03

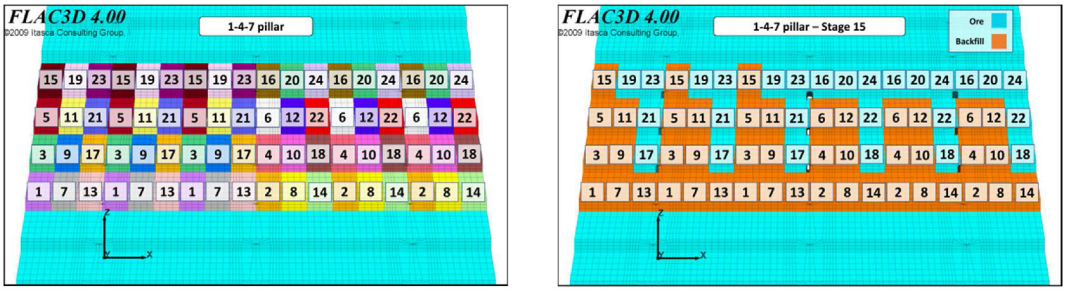

Fig. 3. The 1-4-7 stope pillar method (a) stope extraction sequence numbers (b) layout of mined and unmined stopes in stage 15.

stage will be challenging, and specialized techniques such as destressing might be required.

3.1.2. Footwall and hanging wall

The consequences of instability in the greenstone formation that constitutes both the footwall and hanging wall are different than in the orebody. In the latter, stopes are extracted with the mining advance in the block, and the volume of rock mass at risk becomes nil after 24 stages. The upper and lower sill pillars – while retaining significant volumes of the *BSR* exceeding 0.7 – will also be mined eventually and removed as a potential source of induced seismicity. On the other hand, the footwall and hanging wall will remain in place for the entire life of the mine, and no mining will be implemented there. Hence, any instability in these domains will provide a continuous source of ground control challenges. Furthermore, with the drift and crosscut network excavated in the footwall, the greenstone formation at risk will impact its stability and, therefore, enhanced support installation will be required to keep it functional.

Fig. 5 presents the changing volume of unstable rock mass in the footwall and hanging wall during ore extraction on the four active levels. A first observation is that the volume of unstable rock mass in the host rock is much smaller than that in the orebody. While the latter peaks at approx. 95,000 m^3 in stage 24, the volume in the footwall does not exceed 2640 m^3 and is at a maximum of 3616 m^3 in the hanging wall on a single active or inactive level. The second difference is that the bottom (L1550) and top (L1460) active levels are the ones that carry the largest volumes of unstable rock mass in the footwall and hanging wall, and not the sill pillar levels. However, L1520 and L1490 in these two locations exhibit the same variable trends observed in the orebody. When taken together with the increase in ore at risk in the sill pillars, this trend presents an indication of the wrap-around effect of induced stresses as they are shed from the stopes being mined and channelled into the rock mass – both

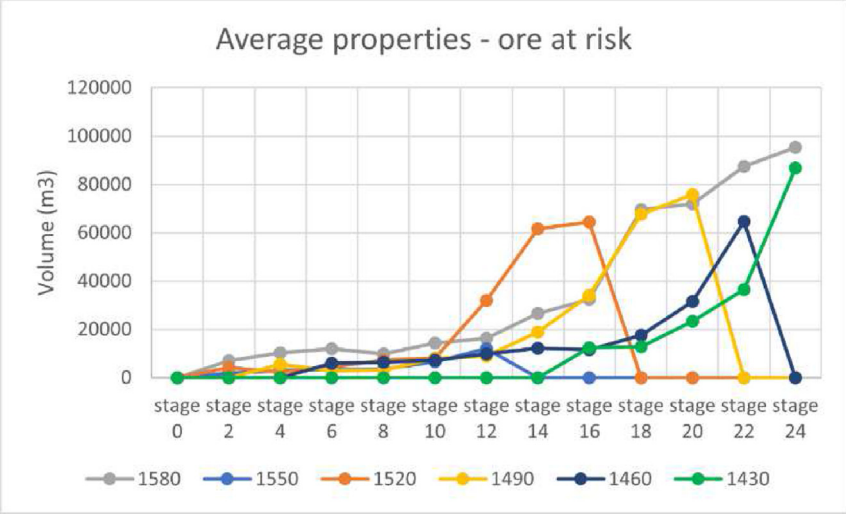

Fig. 4. Volume of orebody with BSR > 0.7 on various levels.

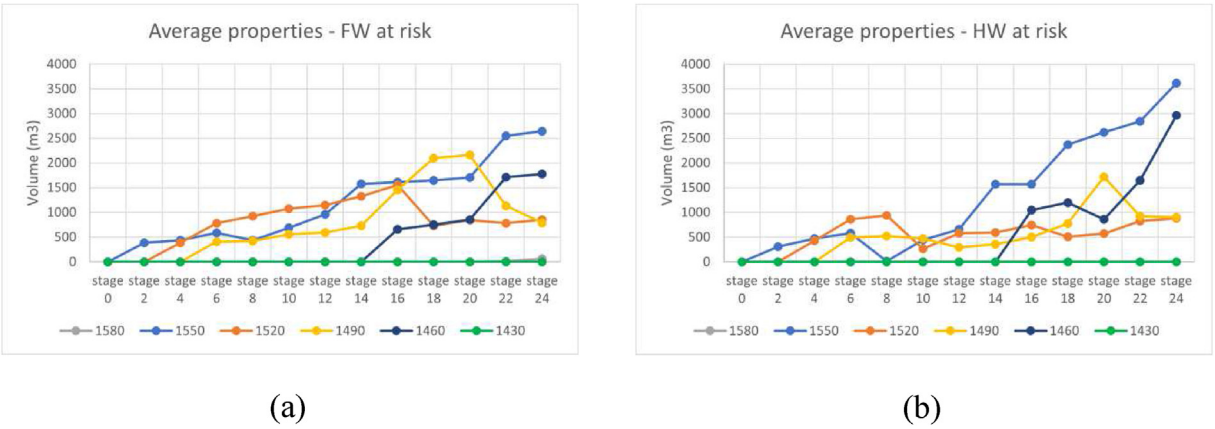

(a) (b)

Fig. 5. Volume of rock mass with BSR > 0.7 on various levels (a) in the footwall and (b) hanging wall within the greenstone formation.

the orebody and host rock – immediately adjacent to the openings.

3.2. Weak and strong greenstone formation

3.2.1. Active level L1520

Two additional simulations were run where the greenstone formation was provided with weak and strong rock mass properties to assess the impact of their variations on instability. All the other geologic formations, including the orebody, retained their initial average properties, as indicated in Table 1. Fig. 6 presents a graphic comparison of the ore at risk with the three sets of properties for the greenstone formation on L1520, while Fig. 7 does the same for the footwall and hanging wall sides.

In the case of the orebody, it is clear that a weak host rock induces further instability in the stope pillars. This is to be expected because the stresses would be transferred from the less competent greenstone formation into the orebody and thus increase the volume of ore with a *BSR* above 0.7. On the other hand, a stronger host rock would attract elevated stresses and relieve the orebody, causing the total volume of ore at risk to decrease. It can also be observed that the largest difference of ore at risk on this level occurs in stage 12, with a 33,000 m^3 change in volume between weak and strong host rock formations. This is the time when extended pillars are formed from L1580 to L1430, and a weak host rock would imply stress shedding to these pillars. In addition, the chart informs the ground control team that the most significant impact of these differences in rock mass properties lasts during stage 10–16. Once the total actual time required to extract the mining block is determined, it can easily be calculated how long this maximum impact, which is spread over seven stages, will last in real time.

Fig. 7 presents the impact of variations on instability in the footwall and hanging wall on this same

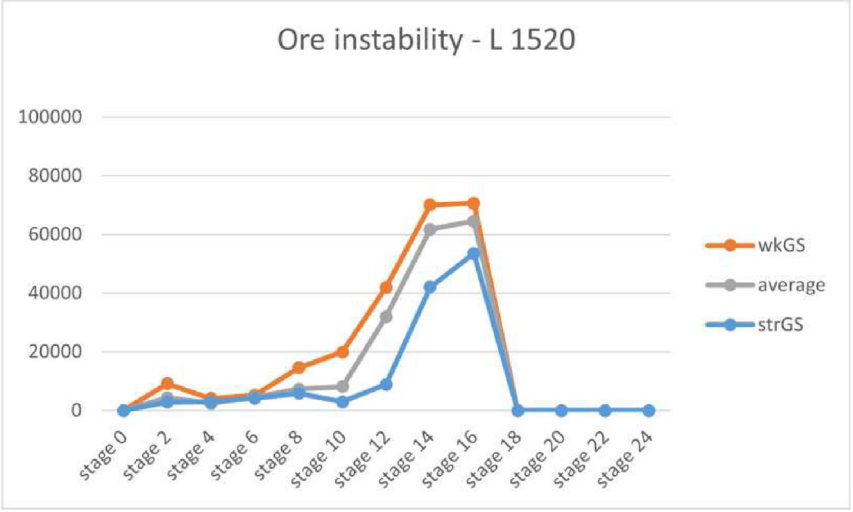

Fig. 6. Volume of orebody with BSR > 0.7 on L1520 with varying host rock mass properties.

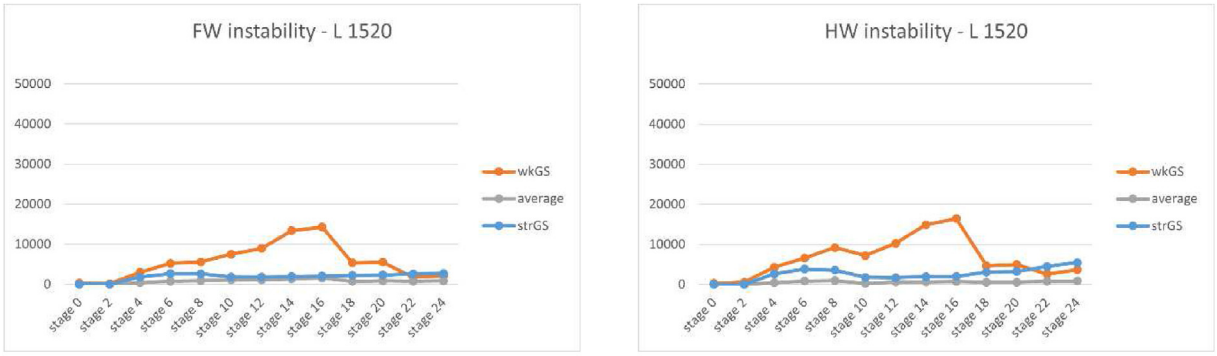

Fig. 7. Volume of rock mass with BSR >0.7 on L1520 (a) in the footwall and (b) hanging wall with varying host rock mass properties.

active level. It can be observed that the maximum volumes in the range of 16,500 m^3 here are much less than the 70,500 m^3 determined in the orebody. However, there are several differences in the volumetric trends for the footwall and hanging wall. Firstly, both the average and strong greenstone properties generate a relatively minor volume of instability there with a maximum of 5500 m^3 compared to 16,500 m^3 for weak properties. Secondly, it would be expected that if weak host rock properties increased instability in the orebody by transferring induced stresses there, they would also decrease the rock mass volume at risk in the greenstone formation.

The explanation for this second observation is relatively simple once it is recalled that the *BSR* is the ratio of deviatoric stress ($\sigma_1-\sigma_3$) to the unconfined compressive strength (UCS_i) of the intact rock. Hence, its value is dependent on both the induced stresses in the numerator and the UCS_i value in the denominator. If stresses are shed to another formation and increase slightly there, the *BSR* could still decrease if the UCS_i value increases significantly in the denominator. In Table 1, the average UCS_i of the host rock is 178 MPa, which decreases to 101 MPa for the weak alternative and increases to 268 MPa for the strong one. Since the *BSR* is dependent on both the deviatoric stress and UCS_i, it would be instructive to examine their impacts separately. The former can be evaluated by plotting the maximum shear stress, which is simply $(\sigma_1-\sigma_3)/2$, and the latter can be read from Table 1, as explained below.

3.2.2. *Overall instability*

Before further analysis into the *BSR* increase in both the orebody and the host rock, the impact of weak and strong properties in the latter should be examined on the overall instability trends. Fig. 8 plots the volume of ore at risk for active levels and

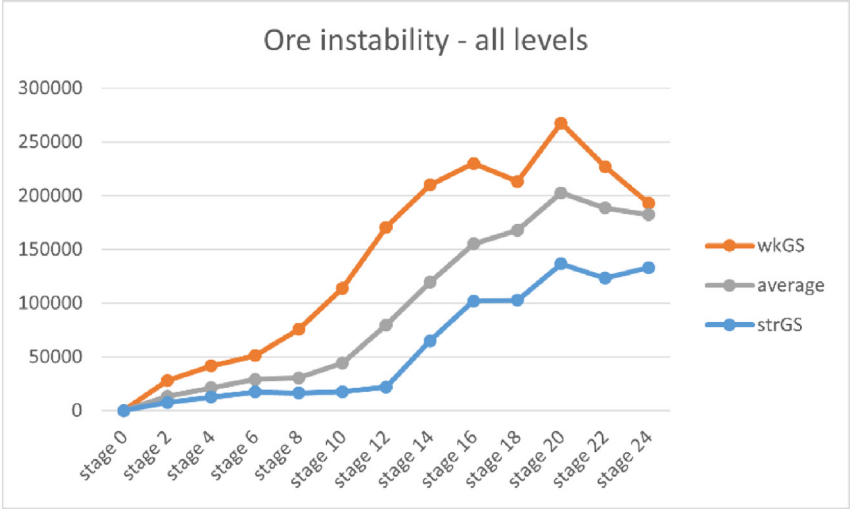

Fig. 8. Volume of orebody with BSR > 0.7 in the entire mining block with varying host rock mass properties.

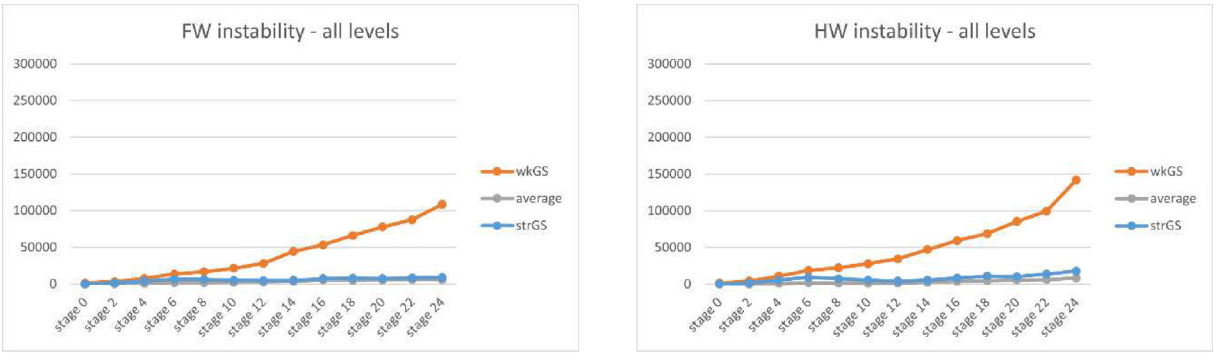

Fig. 9. Volume of rock mass with BSR >0.7 in the entire mining block (a) in the footwall and (b) hanging wall with varying host rock mass properties.

sill pillars for the three sets of properties in the greenstone formation. The trend is almost the same as the one for L1520 in Fig. 6, with the weak host rock inducing maximum instability in the orebody and the largest volumetric difference — almost 150,000 m^3 — observed in stage 12. However, since the chart also plots the ore at risk on L1580 and L1430, the volumes do not converge to zero in stage 24 but move towards values between 133,000 and 193,000 m^3 in the end.

The trend in the overall host rock at risk is plotted in Fig. 9. It shows similarities to the one for L1520 in Fig. 7. Once again, the average and strong properties result in minimal volumes of rock mass at risk while the weak ones generate a continuously increasing trend with a maximum value of 110,000 to 142,000 m^3 in the footwall and hanging wall, respectively.

With the confirmation of larger volumes of instability in both the orebody and the host rock for the weak greenstone properties in the entire mining block, it is obvious that this is not an isolated result that occurs on L1520 only. Hence, by plotting the maximum shear stress and the volume of rock mass above a *BSR* of 0.7, the individual contributions of induced stresses and the UCS_i of the rock can be assessed. In Table 1, the average laboratory strength of the greenstone formation is given at 178 MPa. Since the *BSR* is a ratio of deviatoric stress to UCS_i, it can easily be calculated that the former would need to be 124.6 MPa for a 0.7 threshold. The maximum shear stress is half the deviatoric value, which would therefore be 62.3 MPa for average greenstone formation properties. By comparing the zones above a maximum shear stress of 62.3 MPa for the weak and strong greenstone simulations, the individual contributions of the rock mass properties and UCS_i towards the *BSR* value can be assessed. Specifically, induced stresses and volumes of *BSR* above 0.7 can better be understood when compared to the average baseline properties in the initial simulation. Fig. 10a presents the maximum shear stress readings in the orebody in stage 16 for weak greenstone properties, and Fig. 10b indicates the volume of footwall and

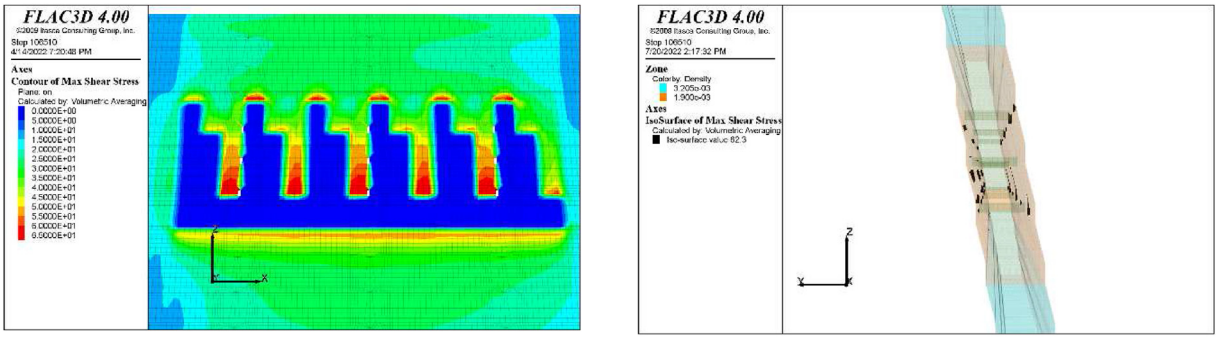

Fig. 10. Maximum shear stress for weak greenstone properties (a) in the orebody (front view) and (b) above 62.3 MPa (dark surfaces) in the footwall and hanging wall (side view) in stage 16.

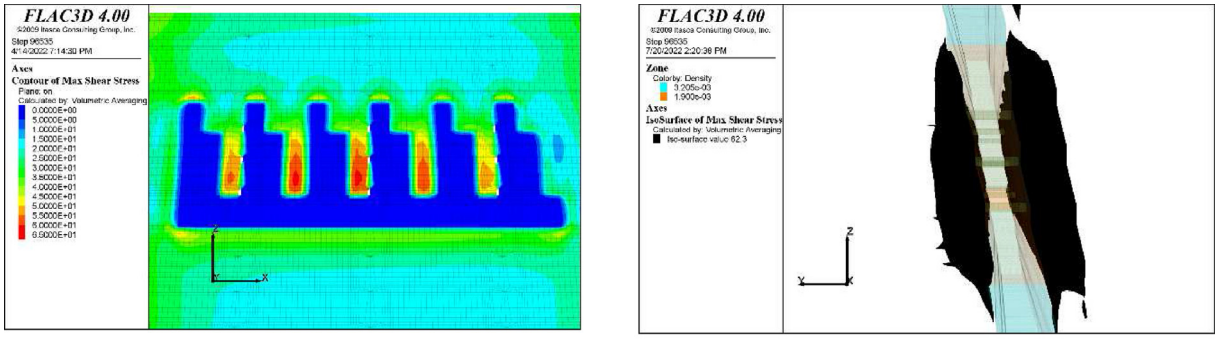

Fig. 11. Maximum shear stress for strong greenstone properties (a) in the orebody (front view) and (b) above 62.3 MPa (dark surfaces) in the footwall and hanging wall (side view) in stage 16.

hanging wall with a maximum shear stress of 62.3 MPa for the same conditions. The latter translates into deviatoric stress of 124.6 MPa and, compared to the weak UCS_i value of 101 MPa, results in a *BSR* of 1.24. From the scale in Fig. 10a, the maximum shear stress in the orebody on L1520 can be approximated to be above 50 MPa, and the volume of host rock above 62.3 MPa appears to be minimal in Fig. 10b.

Fig. 11a and b presents the same results in stage 16 for strong greenstone properties. The maximum shear stress on L1520 in the orebody can once again be approximated to be above 50 MPa (Fig. 11a), which is not significantly different from the previous case. However, regions of the greenstone formation above 62.3 MPa in maximum shear stress are much more voluminous in that they envelop the orebody from the footwall and hanging wall sides (Fig. 11b). In this case, with a UCS_i of 268, the *BSR* in these areas is 0.47.

The strong properties of the host rock channel induced stresses towards the footwall and hanging wall, and away from the orebody, which is to be expected. This is clearly seen in Fig. 11, with voluminous regions of 62.3 MPa in maximum shear stress and slightly lower readings in the orebody. In Fig. 10, the orebody attracts higher shear stresses due to the weak nature of the host rock that exhibits only localized regions of 62.3 MPa. The paradox of the host rock having more voluminous regions of stress-based instability with weak properties can once again be explained by the UCS_i used in the *BSR* formula. Zones in the footwall and hanging wall with a relatively high maximum shear stress of 62.3 MPa are minimal, but the *BSR* volumes are high because a UCS_i of 101 MPa is being used for its assessment. On the other hand, maximum shear stresses of 62.3 MPa are abundant when strong greenstone properties are used, but the *BSR* volumes are low as a UCS_i of 268 is considered in the formulation. This underscores the importance of fully understanding the concepts behind a given instability criterion and the parameters to which it is sensitive.

4. Conclusions

Variations in rock mass properties are an inherent part of structural geology in underground mines. There is abundant literature on methods whereby these can be analyzed, and representative values selected for design purposes or as input for numerical models. There are also practical approaches whereby the impact of these variations on instability at locations of interest can be evaluated. In this study, a typical tabular orebody in the Canadian Shield is modelled in 3D, and the impact of variations in the host rock is assessed quantitively on the orebody, footwall, and hanging wall using the "brittle shear ratio" (*BSR*). It is observed that the volume of ore at risk moves sequentially from one active level to another until all four levels are completely mined, at which point instability moves into the bottom and top sill pillars. The volume of rock mass at risk in the footwall and the hanging wall is much less than in the orebody, but it remains in place even after the mining block has been completely extracted. The charts presenting the results can indicate when, where, and how long instability will be present, allowing ground control measures — such as enhanced support — to be implemented. When the rock mass properties of the greenstone host rock formation are weak, elevated stresses are shed to the orebody and increase the

volume of ore at risk there. However, the volume of footwall and hanging wall at risk also increases due to a lower compressive strength value being used in the *BSR* formula. When the greenstone formation is allocated strong properties, the volume of ore at risk diminishes due to stresses moving into the host rock. The volume of footwall and hanging wall at risk also becomes smaller because of a higher compressive strength value used in the *BSR* formula. In future studies, the authors will examine the impact of variations in the orebody and other geologic formations to develop a comprehensive overview of their impact on instability in the orebody, footwall, and hanging wall.

Ethical statement

The authors state that the research was conducted according to ethical standards.

Funding body

This research was funded by Natural Science and Engineering Research Council of Canada (NSERC) – Discovery Grant Program.

Conflict of interest

The authors declare no conflict of interest.

References

[1] Potvin Y, Hudyma M. Open stope mining practices in Canada. In: Proceedings of the 1989 CIM annual general meeting. Quebec City; 1989. QC, Canada.
[2] Potvin Y, Hudyma M. Open stope mining in Canada. In: Proceedings of MassMin 2000; 2000. p. 661–74. Brisbane, QLD, Australia;.
[3] Villaescusa E. Global extraction sequence in sublevel stoping. In: Proceedings of the 12th MPES conference; 2003. p. 9–17. Kalgoorlie, WA, Australia.
[4] Pakalnis RT, Hughes PB. Sublevel stoping. In: Darling P, editor. SME mining engineering handbook. 3rd ed. Englewood, CO, USA: SME; 2011.
[5] Castro LAM, Bewick RP, Carter TG. An overview of numerical modelling applied to deep mining. In: Azevedo R, editor. Innovative numerical modelling in geomechanics. London, UK: CRC Press, Taylor & Francis Group; 2012.
[6] Board M, Brummer R, Seldon S. Use of numerical modeling for mine design and evaluation. In: Hustrulid WA, Bullock RL, editors. Underground mining methods: engineering fundamentals and international case studies. Littleton, CO, USA: SME; 2001.
[7] Wiles TD. Reliability of numerical modelling predictions. Int J Rock Mech Min Sci 2006;43(3):454–72.
[8] Martin CD, Kaiser PK, McCreath DR. Hoek-Brown parameters for predicting the depth of brittle failure around tunnels. Can Geotech J 1999;36(1):136–51.
[9] Diederichs MS. Instability of hard rock masses: the role of tensile damage and relaxation. Waterloo: University of Waterloo; 1999. PhD thesis.
[10] Kaiser PK, Diederichs MS, Martin CD, Sharpe J, Steiner W. Underground works in hard rock tunnelling and mining. In: Proceedings of the ISRM international symposium; 2000. p. 841–926. Melbourne, VIC, Australia.
[11] Kim BH. Kaiser PK Rock strength characterization for excavations in brittle failing rock. In: Proceedings of the 3rd Canada-US rock mechanics symposium (paper 3948). Toronto, ON: Canada; 2009.
[12] Shnorhokian S, Mitri HS, Moreau-Verlaan L. Stability assessment of stope sequence scenarios in a diminishing ore pillar. Int J Rock Mech Min Sci 2015;74:103–18.
[13] Heidarzadeh S, Saeidi A, Rouleau A. Use of probabilistic numerical modelling to evaluate the effect of geomechanical parameter variability on the probability of open-stope failure: a case study of the Niobec Mine, Quebec (Canada). Rock Mech Rock Eng 2020;53:1411–31.
[14] Heidarzadeh S, Saeidi A, Rouleau A. Evaluation of the effect of geometrical parameters on stope probability of failure in the open stoping method using numerical modeling. Int J Min Sci Technol 2019;29:399–408.
[15] Pelley CW. A study of sequencing strategy for steep, tabular, hardrock orebodies. PhD thesis. Montreal: McGill University; 1994.
[16] Manchuk J. Stope design and sequencing. Edmonton: MS thesis. University of Alberta; 2007.
[17] Bewick RP. Shear rupture of massive brittle rock under constant normal stress and stiffness boundary conditions. Toronto: PhD thesis. University of Toronto; 2013.
[18] Morissette P, Hadjigeorgiou J, Punkkinen AR, Chinnasane D, Sampson-Forsythe A. The influence of mining sequence and ground support practice on the frequency and severity of rockbursts in seismically active mines of the Sudbury Basin. J S Afr Inst Min Metall 2017;117:47–58.
[19] Bouzeran L, Pierce M, Jalbout A, Ruest M. Stoping sequence optimisation at Eleonore Mine based on stress analysis through horizon scale numerical modelling. In: Proceedings of the 9th deep and high stress mining; 2019. p. 253–66. Johannesburg, South Africa.
[20] Kabwe E. Mining sequence deformation and failure behavior analysis in the hanging wall and orebody rock formations; a continuum approach. Geotech Geol Eng 2017;35(4):1453–73.
[21] Handley MF, de Lange JAJ, Essrich F, Banning JA. A review of sequential grid mining method employed at Elandsrand Gold Mine. J S Afr Inst Min Metall 2000;100(3): 157–68.
[22] Jooste Y, Malan DF. Rock engineering aspects of a modified mining sequence in a dip pillar layout at a deep gold mine. J S Afr Inst Min Metall 2015;115:1097–112.
[23] Neindorf LB, Karunatillake GSB. George Fisher Mine – feasibility and construction. In: Proceedings of MassMin 2000; 2000. p. 601–9. Brisbane, QLD, Australia.
[24] Cepuritis PM, Villaescusa E. Back analysis techniques for assessing open stope performance. In: Proceedings of the Australian mining technology conference. NSW, Australia: Hunter Valley; 2006. p. 261–71.
[25] Cepuritis PM, Villaescusa E, Lachenicht R. Back analysis and performance of block A long hole open stopes – Kanowna belle gold mine. In: Proceedings of the 1st Canada-US rock mechanics symposium. Vancouver, BC: Canada; 2007. p. 1431–45.
[26] Grant D, De Kruijff S. Mount Isa mines – 1100 orebody, 35 years on. In: Proceedings of MassMin 2000; 2000. p. 591–600. Brisbane, QLD, Australia.
[27] Beck DA, Sandy MP. Mine sequencing for high recovery in Western Australian mines. In: Proceedings of the 12th MPES conference; 2003. p. 137–44. Kalgoorlie, WA, Australia.
[28] Mgumbwa J, Page A, Human L, Dunn MJ. Managing a change in rock mass response to mining at the Frog's Leg under-ground mine. In: Proceedings of the 8th deep and high stress mining; 2017. p. 917–36. Perth, WA, Australia.
[29] Sjöberg J, Perman F, Quinteiro C, Malmgren L, Dahnér-Lindkvist C, Boskovic M. Numerical analysis of alternative mining sequences to minimise potential for fault slip rockbursting. Min Technol 2012;121(4):226–35.

[30] Kim K, Gao H. Probabilistic approaches to estimating variation in the mechanical properties of rock masses. Int J Rock Mech Min Sci 1995;32(2):111–20.
[31] Sari M. The stochastic assessment of strength and deformability characteristics for a pyroclastic rock mass. Int J Rock Mech Min Sci 2009;46:613–26.
[32] Sari M, Karpuz C, Ayday C. Estimating rock mass properties using Monte Carlo simulation: Ankara andesites. Comput Geosci 2010;36:959–69.
[33] Idris M, Basarir H, Nordlund E, Wettainen T. The probabilistic estimation of rock masses properties in Malmberget mine, Sweden. Electron J Geotech Eng 2013;18:269–87.
[34] Wang Y, Aladejare AE. Evaluating variability and uncertainty of geological strength index at a specific site. Rock Mech Rock Eng 2016;49:3559–73.
[35] Hoek E. Reliability of the Hoek–Brown estimates of rock mass properties and their impact on design. Int J Rock Mech Min Sci 1998;35:63–8.
[36] Marinos P, Hoek E, Marinos V. Variability of the engineering properties of rock masses quantified by the geological strength index: the case of ophiolites with special emphasis on tunnelling. Bull Eng Geol Environ 2006;65:129–42.
[37] Sari M. Incorporating variability and/or uncertainty of rock mass properties into GSI and RMi systems using Monte Carlo method. In: Lollino G, Giordan D, Thuro K, Carranza-Torres C, Wu F, Marinos P, et al., editors. Engineering geology for society and territory. Applied geology for major engineering projects, Part XIV, vol. 6. Switzerland: Springer International Publishing; 2015. Paper 152.
[38] Morelli GL. Variability of the GSI index estimated from different quantitative methods. Geotech Geol Eng 2015;33:983–95.
[39] Barla G, Scavia C, Antonellis M, Garascio M. Characterization of rock mass by geostatistical analysis at the Masua Mine. In: Proceedings of the 6th ISRM congress. Montreal, QC: Canada; 1987. p. 777–86.
[40] Cai M. Rock masses characterization and rock property variability considerations for tunnel and cavern design. Rock Mech Rock Eng 2011;44:379–99.
[41] Mazraehli M, Zare S. An application of uncertainty analysis to rock mass properties characterization at porphyry copper mines. Bull Eng Geol Environ 2020;79:3721–39.
[42] Esmaieli K, Hadjigeorgiou J, Grenon M. Estimating geometrical and mechanical REV based on synthetic rock mass models at Brunswick Mine. Int J Rock Mech Min Sci 2010;47:915–26.
[43] Sari M. Determination of representative elementary volume (REV) for jointed rock masses exhibiting scale-dependent behavior: a numerical investigation. Int J Geo-Engineering 2021;12:34.
[44] Heidarzadeh S, Saeidi A, Lavoie C, Rouleau A. Geomechanical characterization of a heterogenous rock mass using geological and laboratory test results: a case study of the Niobec Mine, Quebec (Canada). SN Appl Sci 2021;3(640).
[45] Harrison JP. Challenges in determining rock mass properties for reliability-based design. In: Proceedings of the 7th international symposium on geotechnical safety and risk; 2019. p. 35–44. Taipei, Taiwan.
[46] Fattahi H, Varmazyari Z, Babanouri N. Feasibility of Monte Carlo simulation for predicting deformation modulus of rock mass. Tunn Undergr Space Technol 2019;89:151–6.
[47] Aladejare AE, Wang Y. Estimation of rock mass deformation modulus using indirect information from multiple sources. Tunn Undergr Space Technol 2019;85:76–83.
[48] Tiwari G, Pandit B, Madhavi Latha G, Babu GLS. Probabilistic analysis of tunnels considering uncertainty in peak and post peak strength parameters. Tunn Undergr Space Technol 2017;70:375–87.
[49] Behnia M, Cheraghi Seifabad M. Stability analysis and optimization of the support system of an underground power-house cavern considering rock mass variability. Environ Earth Sci 2018;77:645.
[50] Aladejare AE, Wang Y. Evaluation of rock property variability. Georisk 2017;11(1):22–41.
[51] Małkowski P, Niedbalski Z, Balarabe T. A statistical analysis of geomechanical data and its effect on rock mass numerical modeling: a case study. Int J Coal Sci Tech 2021;8(2):312–23.
[52] Stavropoulou M, Exadactylos G, Saratsis G. A combined three-dimensional geological–geostatistical–numerical model of underground excavations in rock. Rock Mech Rock Eng 2007;40(3):213–43.
[53] Jendrys M, Duzy S, Dyduch G. Analysis of stress-strain states in the vicinity of mining excavations in a rock mass with variable mechanical properties. Energies 2020;13:5567.
[54] Idris MA, Saiang D, Nordlund E. Numerical analyses of the effects of rock mass property variability on open stope stability. In: Proceedings of the 45th US rock mechanics/geomechanics symposium – ARMA (Paper 11-297). San Francisco, CA, United States.
[55] Idris MA, Saiang D, Nordlund E. Consideration of the rock mass property variability in numerical modelling of open. In: Bergmekanikdag; 2012. p. 111–23. Stockholm, Sweden.
[56] Idris MA, Saiang D, Nordlund E. Probabilistic analysis of open stope stability using numerical modelling. Int J Min Miner Eng 2011;3(3):194–219.
[57] Idris MA, Saiang D, Nordlund E. Stochastic assessment of pillar stability at Laisvall mine using artificial neural network. Tunn Undergr Space Technol 2015;49:307–19.
[58] Saeidi A, Heidarzadeh S, Lalancette S, Rouleau A. The effects of in situ stress uncertainties on the assessment of open stope stability: case study at the Niobec Mine, Quebec (Canada). Geomech Energ Env 2021;25:100194.
[59] Shnorhokian S, Mitri HS, Moreau Verlaan L. Influence of rockmass property variations on pre-mining stresses: a case study. In: Proceedings of the 68th Canadian geotechnical conference – GéoQuebec 2015, Québec City (QC); 2015. September 20-23. Paper No 348.
[60] Shnorhokian S. 3D volumetric analysis of rock mass instability in various stope sequences. In: Proceedings of the V Seminario Peruano de Geoingeniería – ISRM Peru; 2021. p. 186–94. Lima, Peru.
[61] Shnorhokian S, Mitri HS, Thibodeau D. A methodology for calibrating numerical models with a heterogeneous rock mass. Int J Rock Mech Min Sci 2014;70:353–67.
[62] Brown ET, Hoek E. Trends in relationships between measured in-situ stresses and depth. Int J Rock Mech Min Sci 1978;15(4):211–5.
[63] Arjang B, Herget G. In-situ ground stresses in the Canadian hard rock mines: an update. Int J Rock Mech Min Sci 1997;34(15):1–15.